

Electromagnetic Signals of Inelastic Dark Matter Scattering

Masha Baryakhtar,¹ Asher Berlin,¹ Hongwan Liu,^{1,2} Neal Weiner¹

¹*Center for Cosmology and Particle Physics, Department of Physics, New York University, New York, NY 10003, USA*

²*Department of Physics, Princeton University, Princeton, NJ 08544, USA*

E-mail: mbaryakhtar@nyu.edu, ajb643@nyu.edu, hongwanl@princeton.edu,
neal.weiner@nyu.edu

ABSTRACT: Light dark sectors in thermal contact with the Standard Model naturally produce the observed relic dark matter abundance and are the targets of a broad experimental search program. A key light dark sector model is the pseudo-Dirac fermion with a dark photon mediator. The dynamics of the fermionic excited states are often neglected. We consider scenarios in which a nontrivial abundance of excited states is produced and their subsequent de-excitation yields interesting electromagnetic signals in direct detection experiments. We study three mechanisms of populating the excited state: a primordial excited fraction, a component up-scattered in the sun, and a component up-scattered in the Earth. We find that the fractional abundance of primordial excited states is generically depleted to exponentially small fractions in the early universe. Nonetheless, this abundance can produce observable signals in current dark matter searches. MeV-scale dark matter with thermal cross sections and higher can be probed by down-scattering following excitation in the sun. Up-scatters of GeV-scale dark matter in the Earth can give rise to signals in current and upcoming terrestrial experiments and X-ray observations. We comment on the possible relevance of these scenarios to the recent excess in XENON1T.

Contents

1	Introduction	1
2	Model Space	2
3	Excited States from the Early Universe	5
4	Excited States from the Sun	10
5	Excited States from the Earth	17
6	Discussion	19

1 Introduction

Over the past two decades, the model space of WIMP-like dark matter (DM) has expanded dramatically. While canonical WIMPs with TeV-scale masses remain an attractive class of models, great attention has turned to sectors with a broader range of interactions and lighter states. The cosmological evolution and experimental signatures often differ significantly from traditional WIMP scenarios.

One such difference is the presence of inelastic scattering. The existence of an excited state χ^* of the χ DM particle can dramatically alter the energy spectrum in direct detection experiments through endothermic [1] or exothermic scattering processes from long-lived states [2–5]. In particular, the introduction of a new scale, $\delta = m_{\chi^*} - m_{\chi}$ changes the kinematics of processes at or below the mass splitting scale. Decays of the excited state can have profound implications for direct [6–8], indirect, and accelerator signals [9–13].

Another important change has been the introduction of new, light mediators between the dark sector and the Standard Model (SM) [14]. In models with dark photons, in particular, very light (\sim MeV) thermal DM is allowed.

These two modifications are connected. Light Dirac fermion DM is in severe conflict with measurements of the CMB if it can annihilate at the time of recombination [15–17]. However, a pseudo-Dirac fermion escapes the CMB constraints if only the ground state χ has a significant abundance. Thus, a broad class of light DM models necessarily introduces both of these components.

If the splitting is present, the elastic scattering process is highly suppressed in light DM models with dark photon mediators. As a consequence, understanding the possible presence of these excited states and their signals is imperative.

For MeV mass DM particles, there are two natural scales to consider. The first is an $\mathcal{O}(1) \sim \mathcal{O}(\text{MeV})$ splitting in the dark sector, which decouples the excited states from questions of direct detection. However, the splitting breaks a symmetry of the theory, and has a scale generally smaller than the other scales in the theory. Thus a second possibility is splittings in the $\alpha/4\pi \times \mathcal{O}(\text{MeV}) \sim \mathcal{O}(\text{keV})$ range, which change the signatures of direct detection experiments. While the nuclear signals of these excited states have been studied [5, 18, 19], the electronic signals are relatively unexplored.

While MeV-scale excitations typically decay promptly into e^+e^- pairs, keV excitations are potentially long-lived and of the appropriate energy scale to impact direct detection. It is this latter case that we consider in this paper, with a particular emphasis on electronic signals of χ^* down-scattering in direct detection experiments. A systematic study of this parameter space and cosmological history, including signals of nuclear recoils from primordial states, is expected to soon appear in [20].

Elastic WIMP recoils of light particles typically deposit $\sim v^2 m_\chi \sim 10 \text{ eV}$ of energy [21–23]. Such small energies are currently observable with precision experiments with small target masses [24, 25] or large targets at the expense of less background rejection [26–28]. Inelastic scatters of keV energies allows one to consider limits in energy ranges of the experiment where one can properly fiducialize, including in the current world-leading xenon experiments [26, 29, 30]. In this paper, we shall show that ongoing experiments are sensitive to thermal relics through their inelastic scattering. Recently, the XENON1T collaboration has reported an excess of electron recoil events [30]. We shall see that the scenarios we shall consider provide possible explanations to this excess and predict future testable experimental consequences.

The layout of this paper is as follows: in Sec. 2, we present the parameter space of the model in question. In Secs. 3–5, we consider various possible sources of excited states, including the early universe, the Sun, and the Earth, the resulting implications of these states in direct detection experiments. We consider other terrestrial and astrophysical signatures, and make a connection to the 3.5 keV line observed from nearby galaxies and galaxy clusters as well as future laboratory experiments. Finally, we conclude in Sec. 6.

2 Model Space

We consider models of DM with excited states. Such models are common in particle physics, and span a wide range of mass. Since we will be interested in the energy deposition of these excited states into direct detection experiments, we will need a means of both producing and de-exciting these states. We focus on thermal relics, which can make up all of the DM, or can be a subcomponent.

We shall operate within a specific framework of thermal relics with interactions mediated by a dark photon. The ingredients of the model under question combines features discussed broadly in the literature over more than a decade [31–38]. We consider a light DM particle, coupled to a massive dark photon which is kinetically mixed with the Standard Model photon. We consider the DM to be a pseudo-Dirac fermion χ and χ^* split by an amount δ . We further

consider a dipole moment allowing transitions between the DM. The interaction Lagrangian is

$$\mathcal{L} \supset \frac{\epsilon}{2} F_{\mu\nu} F'^{\mu\nu} + i e_D A'_\mu \bar{\chi}^* \gamma^\mu \chi + \frac{1}{\Lambda_d} \bar{\chi}^* \sigma^{\mu\nu} \chi F_{\mu\nu}, \quad (2.1)$$

where $e_D = \sqrt{4\pi\alpha_D}$ is the dark photon gauge coupling. The dark photon and dipole can each allow for transitions between the ground and excited DM state. Both vector interactions as well as dipole operators are off-diagonal between the mass eigenstates of the pseudo-Dirac fermion.

We first consider the processes arising from the presence of the dark photon. The up- and down-scattering cross section is parametrized by the cross section in the elastic limit. For a target T with charge Z_T this is simply

$$\sigma_T = \frac{16\pi Z_T^2 \alpha \alpha_D \mu^2 \epsilon^2}{m_{A'}^4} = \frac{16\pi Z_T^2 \alpha \mu^2 y}{m_\chi^4}, \quad (2.2)$$

where μ is the reduced mass of the target and DM particles and the variable

$$y \equiv \epsilon^2 \alpha_D (m_\chi/m_{A'})^4 \quad (2.3)$$

is a commonly used parameterization of the DM couplings [13]. $\mu = \mu_{\chi T}$ is the reduced mass of the χ -target system, and subscripts are suppressed when the meaning is clear. When the kinematics are unimportant, this characterizes the overall process for up- and down-scattering. When the splitting is significant compared to the overall kinematics, the width of the recoil energy distribution is corrected compared to the elastic case

$$\Delta E_R = \frac{2\mu^2 v^2 \sqrt{1 \pm \frac{2\delta}{\mu v^2}}}{M_T} = \Delta E_{R,\text{elastic}} \sqrt{1 \pm \frac{2\delta}{\mu v^2}}, \quad (2.4)$$

where $+$ is for exothermic and $-$ for endothermic inelastic scattering and v is the DM velocity. This corrects the overall scattering cross section

$$\sigma_{T,\text{inel}} = \sigma_{T,\text{elastic}} \sqrt{1 \pm \frac{2\delta}{\mu v^2}}, \quad (2.5)$$

(see, e.g., Refs. [1, 2, 4, 5]).

Decays of excited states can occur through the dark photon; in the parameter range we consider, the lifetime is longer than the age of the universe [2, 3]. Only once the splitting is $\mathcal{O}(\text{MeV})$ and de-excitations into e^+e^- pairs are allowed, does the lifetime become short.

The higher-dimensional dipole operator in Eq. (2.1) can also result in up- and down-scattering, and scenarios involving this have been discussed previously [7, 8]. For our studies, the dipole will be essential for scenarios with short decay lifetimes. The excited state decays at a rate of

$$\tau^{-1} \sim \pi \delta^3 / \Lambda_d^2 \sim \text{sec}^{-1} \times \left(\frac{\delta}{\text{keV}} \right)^3 \left(\frac{\text{TeV}}{\Lambda_d} \right)^2. \quad (2.6)$$

The scale of the dipole moment is important in determining the possible source of the excited states. In principle, a dark photon-interacting thermal relic need have no dipole operator with electromagnetism at all. A Planck-suppressed dipole operator (i.e., $\Lambda_d \sim M_{\text{pl}}$) does not mediate a decay over the age of the universe for $\delta \lesssim \text{MeV}$. Thus, a natural starting point would be to consider excited states which are produced primordially and are stable on cosmological timescales, e.g. [2, 3].

In the presence of a larger dipole moment (or another means of decay), the primordial excited abundance is depleted and more local production mechanisms become important. For instance, inelastic up-scattering of DM on targets nearby earth can regenerate a local flux of excited states. The Sun is a natural possibility, given its (relatively) high temperature. The Earth is also a possibility, if the kinetic energy of the DM is large enough. For the Sun to facilitate a signal, the χ^* lifetime must be approximately $1 \text{ AU}/v_0 \sim 10^6 \text{ sec}$ in order to make it to the Earth, where v_0 is the DM velocity dispersion. If χ^* is accelerated from a solar scattering as we shall consider, lifetimes can be a bit shorter, but not in a way that qualitatively changes the picture. For up-scattering in the Earth, the lifetime can be much shorter. Indeed, scenarios with very short ($\sim 100 \mu\text{sec}$) lifetimes have been considered [7]. We will focus on scenarios where the entire Earth is a source of excited states, and thus lifetimes greater than $r_{\text{earth}}/v_0 \sim 100 \text{ sec}$. These requirements broadly are satisfied for $\Lambda_d \gtrsim (10 - 100) \text{ TeV}$. Given that radiative dipoles are typically suppressed by $e m_f$, this is a relatively mild constraint.

Since we will be focused on Xenon signals of such deexcitations and decays, let us take a moment to describe our event rates. Given the ongoing searches for light DM in electron recoils, there has been incredible progress in understanding the ionization rates from DM scattering, e.g., Refs. [21–23, 39, 40]. For ionization of electrons from the elastic scattering of slow-moving DM heavier than an MeV, the momentum transfer is $q \sim m_e v_e$, where the typical electron velocity is $v_e \sim \alpha$. Thus, in order to achieve $\gtrsim \text{keV}$ electron recoil energies above threshold in xenon detectors, one must go well away from the peak of the electron form factor in order to take advantage of the large electron momenta close to the nucleus. In contrast, the scenarios we shall consider in this work involve down-scattering with sizable splittings $\delta \gtrsim \text{keV} \gg \alpha^2 m_e$, such that $q \sim (m_e \delta)^{1/2}$ and the recoil energy is peaked at δ . In other words, the primary support of the process comes from the peak of the electron form factor, and hence, the electron momentum does not play a major role in the scatterings we consider. We estimate the event rates in a xenon detector by assuming the $n = 4, 5$ orbitals are accessible and populated by “free” electrons, and ignore the $n = 1, 2, 3$ orbitals, which are more tightly bound. We expect this to be a reasonable approximation for mass splittings $\delta \gtrsim \text{keV}$ and anticipate $\mathcal{O}(1)$ corrections; a more precise study is warranted in future work.

Having laid out the basic tools for studying the electromagnetic signals of inelastic DM scatters, we are now in a position to consider the actual signals. We will consider three distinct sources of excited states: primordial abundances, excitations from solar reflection, and up-scatterings in the Earth. The signals of each of these will be different and provide different signal constraints.

3 Excited States from the Early Universe

The high densities and temperatures of the early universe provide an efficient means to generating a cosmologically stable χ^* abundance. If DM was part of a thermal bath in the primordial universe, chemical equilibrium drives the relative abundances of χ and χ^* to comparable values. This is indeed the case in standard cosmologies of thermal relics in which DM was once in equilibrium with ordinary matter. At much later times, typically once the temperature is much smaller than the mass splitting δ , the relative abundance of χ^* (compared to χ) is exponentially suppressed and freezes out. Thus, estimating the primordial fraction of χ^* at late times requires tracking the cosmological evolution across the periods of $\chi, \chi^* \leftrightarrow$ SM chemical and kinetic decoupling, as well as the period of $\chi \leftrightarrow \chi^*$ decoupling. In the following discussion, we give simple analytic expressions for the rates of these various processes.

Within the context of Eq. (2.1), DM can maintain chemical equilibrium with the SM bath through coannihilations to electromagnetically charged SM particles f , as mediated by the dark photon, $\chi\chi^* \leftrightarrow A' \leftrightarrow ff$. For temperatures $T \ll m_{A'}$, this process is dominated by the exchange of an off-shell A' . The total comoving $\chi + \chi^*$ density is dictated by the temperature at which these coannihilations decouple. If this occurs at a temperature much greater than the mass splitting δ , the rate for such processes scales as $\sigma v \sim \alpha y/m_\chi^2$. The conserved $\chi + \chi^*$ comoving density is then consistent with observations of the DM energy density provided that $\sigma v \sim 1/(T_{\text{eq}} m_{\text{pl}})$, where $T_{\text{eq}} \sim 0.8$ eV is the temperature at matter-radiation equality and m_{pl} is the Planck mass, which is equivalent to

$$y \sim 10^{-10} \times \left(\frac{m_\chi}{100 \text{ MeV}} \right)^2. \quad (3.1)$$

After chemically decoupling from the SM, χ and χ^* remain chemically coupled to each other through $\chi^*\chi^* \leftrightarrow \chi\chi$ and $\chi^*f \leftrightarrow \chi f$, where the latter process also enforces kinetic equilibrium between the dark sector and the SM. Neither process alters the total $\chi + \chi^*$ number, but each drives the relative number density to the equilibrium value $n_{\chi^*}/n_\chi \sim e^{-\delta/T_\chi}$, where T_χ is the temperature of the $\chi + \chi^*$ bath. Once χ and χ^* chemically decouple from each other, the primordial comoving abundance of the excited state χ^* is no longer depleted by annihilation or scattering processes.

The DM temperature T_χ is governed by the temperature of kinetic decoupling $T_{\text{kin}} \ll m_\chi$, which is in turn dictated by DM-electron down-scattering $\chi^*e \leftrightarrow \chi e$ for $m_\chi \lesssim \text{GeV}$. For $m_\chi \gg \text{MeV}$, $T \lesssim T_{\text{kin}}$ occurs well after χ, χ^* become non-relativistic and chemically decouple from the SM, due to the enhanced abundance of electrons compared to DM particles at early times. In the limit that $m_e \ll T \ll m_{A'}$, the thermally-averaged rate for $\chi^*e \leftrightarrow \chi e$ is

$$\Gamma_{\chi e} \simeq \frac{360 \zeta(5)}{\pi} \frac{\alpha \alpha_D \epsilon^2 T^5}{m_{A'}^4}. \quad (3.2)$$

At much lower temperatures, $T \ll m_e$, $\Gamma_{\chi e}$ is exponentially suppressed, due to the dwindling electron abundance. We estimate T_{kin} as the temperature at which $\Gamma_{\chi e}$ drops below the rate

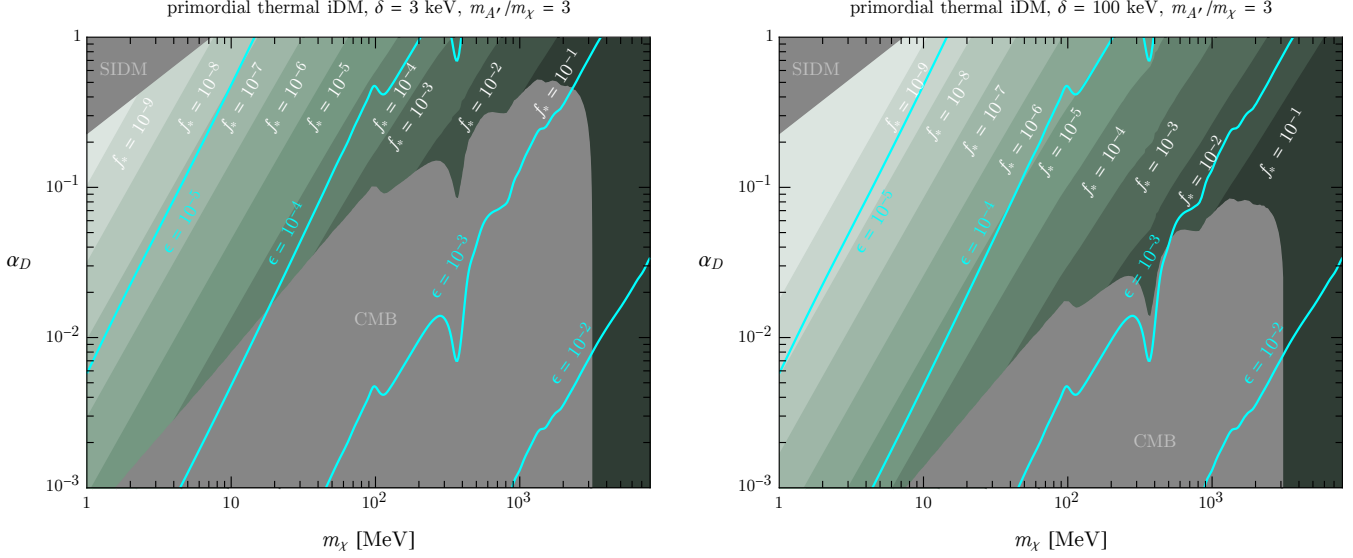


Figure 1: The fraction f_* of dark matter that is composed of excited states (shaded green) as a function of dark matter mass m_χ and dark sector coupling α_D for $m_{A'} = 3m_\chi$ and various values of the $\chi^* - \chi$ mass splitting, $\delta = 3$ keV (left) and 100 keV (right). For each point in parameter space, we fix the kinetic mixing parameter ϵ such that the abundance of χ agrees with the observed dark matter energy density (cyan). Shown in gray are regions excluded by elastic self-scattering of dark matter [12, 41] and distortions of the CMB from late-time annihilations [42].

of Hubble expansion H . For $T \lesssim T_{\text{kin}}$, the DM temperature evolves independently of the SM plasma as $T_\chi \sim T^2/T_{\text{kin}}$. In most of the parameter space that we investigate, kinetic decoupling occurs near or slightly below the electron mass threshold.

Even at temperatures well below the electron threshold, χ and χ^* can remain in chemical equilibrium through DM-DM scattering $\chi^*\chi^* \leftrightarrow \chi\chi$, which is independent of ϵ . Assuming that χ and χ^* are chemically coupled, $n_{\chi^*} \sim e^{-\delta/T_\chi} n_\chi$. The corresponding thermally-averaged rate is roughly

$$\Gamma_{\chi^*\chi} \simeq e^{-\delta/T_\chi} n_\chi \frac{2^{5/2} \pi \alpha_D^2 m_\chi^{3/2}}{m_{A'}^4} \max\left(\frac{2}{\pi} T_\chi, \delta\right)^{1/2}. \quad (3.3)$$

We denote the DM temperature at which $\Gamma_{\chi^*\chi} \sim H$ as $T_{\chi\chi^*}$, which we evaluate numerically. Since $\chi^*e \leftrightarrow \chi e$ also enforces $\chi - \chi^*$ chemical equilibrium, the DM temperature of $\chi - \chi^*$ chemical decoupling is $T_{\chi, \text{chem}} \sim \min(T_{\text{kin}}, T_{\chi\chi^*})$ and is thus controlled by whichever process, $\chi^*e \leftrightarrow \chi e$ or $\chi^*\chi^* \leftrightarrow \chi\chi$, decouples last. Assuming that χ makes up the dominant component of the DM abundance at late times, the number density n_χ in the expression above corresponds to $n_\chi \sim T_{\text{eq}} T^3/m_\chi$. If χ^* is cosmologically stable, its late-time fractional abundance is then

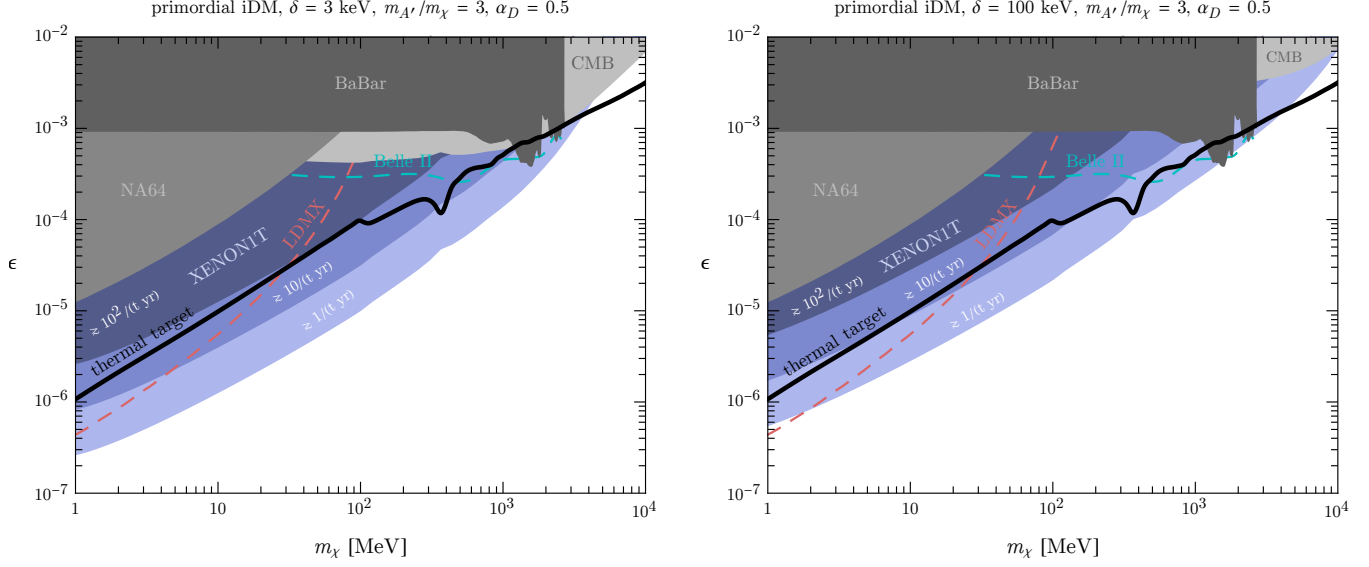


Figure 2: In blue, the event yield at XENON1T from down-scattering of a primordial excited pseudo-Dirac dark matter subcomponent as a function of ϵ and m_χ , for $\alpha_D = 0.5$, $m_{A'}/m_\chi = 3$, and various choices of the mass splitting, $\delta = 3$ keV (left) and $\delta = 100$ keV (right). Throughout, we assume that χ makes up the entirety of the dark matter abundance; along the black contours, the thermal abundance of χ is consistent with the observed dark matter energy density. Also shown are regions excluded by recent missing energy/momentum searches at NA64 [43] and BaBar [44] (solid gray), as well as the projected sensitivities of searches for similar signals at LDMX and Belle II (dashed) [45–48]. Exclusions derived from distortions of the CMB anisotropies are also shown (solid gray) [42].

approximated by

$$f_* \equiv \frac{n_{\chi^*}}{n_\chi + n_{\chi^*}} \simeq e^{-\delta/T_{\chi,\text{chem}}} . \quad (3.4)$$

Ignoring the m_χ -dependence of $T_{\text{kin}} \sim m_e$ and taking $T_{\chi,\text{chem}} \lesssim \delta$, f_* then scales as

$$\begin{aligned} f_* &\sim \frac{m_\chi^{7/2}}{\alpha_D^2 (T_{\chi,\text{chem}} \delta)^{1/2}} \frac{(m_{A'}/m_\chi)^4}{m_e^{1/2} T_{\text{eq}} m_{\text{pl}}} \\ &\sim \text{few} \times 10^{-4} \times \left(\frac{m_\chi}{100 \text{ MeV}} \right)^{7/2} \left(\frac{\alpha_D}{0.5} \right)^{-2} \left(\frac{\delta}{\text{keV}} \right)^{-1} \left(\frac{T_{\chi,\text{chem}}}{\delta} \right)^{-1/2} \left(\frac{m_{A'}/m_\chi}{3} \right)^4 \end{aligned} \quad (3.5)$$

for $m_\chi \sim \mathcal{O}(\text{MeV})$, where the ratio $T_{\chi,\text{chem}}/\delta \lesssim 1$ grows logarithmically with increasing m_χ .

For DM masses well below the GeV-scale, the remaining fractional abundance of excited states χ^* is typically very small, $f_* \ll 1$. The dependence of f_* on various parameters is shown in Fig. 1, in which we vary ϵ as a function of α_D and m_χ by fixing the late-time abundance of

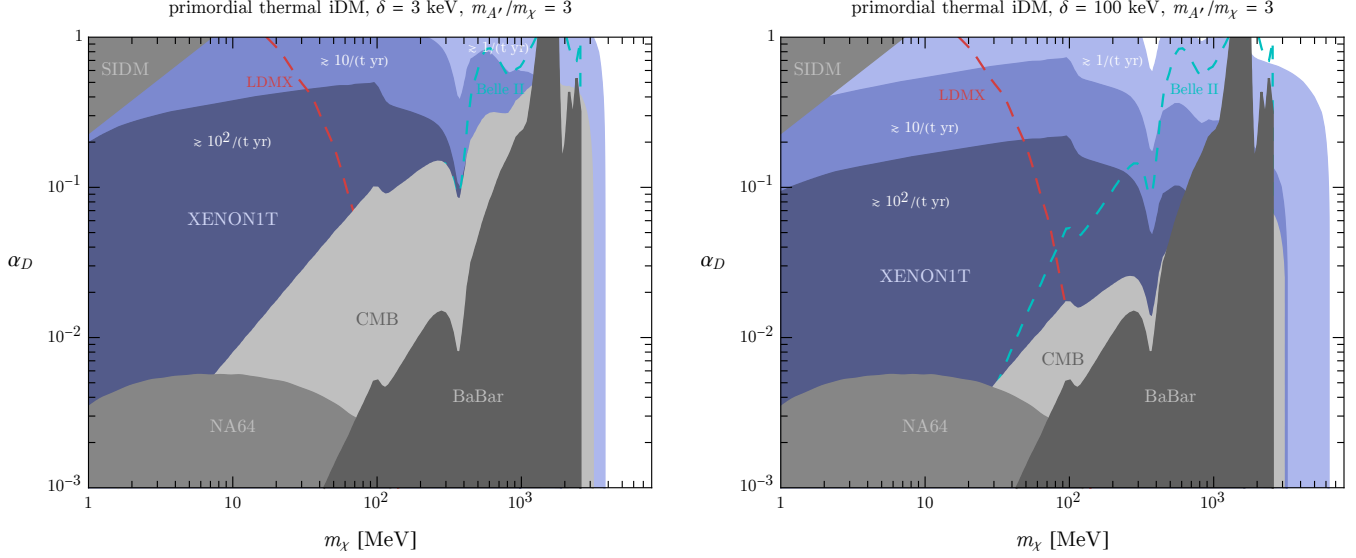


Figure 3: As in Fig. 2, but now in the $\alpha_D - m_\chi$ plane. At each point in parameter space, the value of ϵ is fixed such that χ freezes out with an abundance that is consistent with the observed dark matter energy density, as in Fig. 1.

χ to the observed DM energy density. From Eq. (3.1), this corresponds to

$$\epsilon \sim 10^{-4} \times \left(\frac{m_\chi}{100 \text{ MeV}} \right) \left(\frac{m_{A'}/m_\chi}{3} \right)^2 \left(\frac{\alpha_D}{0.5} \right)^{-1/2}. \quad (3.6)$$

This “thermal target” is also shown as the black contours in the $\epsilon - m_\chi$ parameter space of Fig. 2. As discussed above, this is driven by $\chi\chi^* \leftrightarrow ff$ freeze-out, and in our numerical analysis, we include the effect of hadronic resonances and final states [10]. For smaller α_D or larger m_χ , the ability to deplete the primordial χ^* abundance diminishes, leading to an increased primordial excited state fraction f_* . For $m_\chi \gtrsim \text{few} \times \text{GeV}$, χ^* constitutes an $\mathcal{O}(1)$ fraction of the DM density.

For mass splittings $\delta \gtrsim 2m_e$, the dark photon induced decay $\chi^* \rightarrow \chi + 2e$ may deplete the remaining χ^* abundance to completely negligible levels [2, 3]. However, for $\delta \ll m_e$, in the absence of an additional dipole-type interaction, the only kinematically allowed decays are $\chi^* \rightarrow \chi + 3\gamma$ and $\chi^* \rightarrow \chi + 2\nu$, with a corresponding lifetime that is cosmologically stable. In this case, the primordial χ^* fraction generically survives to late times, potentially giving rise to detectable signatures in cosmological and terrestrial observations.

Near the time of recombination, the primordial abundance of χ^* facilitates late time coannihilations to SM particles, depositing energy into the SM plasma and leading to small distortions in the CMB anisotropies. This process is suppressed by the small residual fraction f_* , but is compensated by the large number density of χ for $m_\chi \ll \text{GeV}$. The resulting energy injected into the SM plasma is strongly constrained by Planck observations, leading

to $f_* \sigma v \lesssim \text{pb} \times (m_\chi/60 \text{ GeV})$ for electromagnetic final states [42]. The corresponding cross section for coannihilations to leptonic final states is

$$\sigma v(\chi\chi^* \rightarrow \ell\ell) \simeq \frac{16\pi \alpha \alpha_D \epsilon^2 m_\chi^2}{m_{A'}^4} . \quad (3.7)$$

The resulting Planck bound is shown in gray in Figs. 1-3. As shown explicitly in Fig. 1, this is most constraining for $m_\chi \sim \text{GeV}$, in which case $f_* \gtrsim \mathcal{O}(10^{-1})$. For much larger masses, f_* saturates at $f_* \sim \mathcal{O}(1)$, while the DM number density falls as $\sim 1/m_\chi$, leading to a weakening of the bounds.

The consideration of DM halo shapes and merging galaxy clusters constrain the rate for DM elastic scattering to be $\sigma(\chi\chi \rightarrow \chi\chi)/m_\chi \lesssim 10 \text{ cm}^2/\text{g}$ [41]. Such limits therefore restrict large values of α_D and are especially relevant at small DM masses, as shown in gray in Figs. 1 and 3. In scenarios involving $f_* \ll 1$ and mass splittings greater than the typical DM kinetic energy, the dominant process at small masses arises from elastic scattering $\chi\chi \rightarrow \chi\chi$ that is radiatively induced by A' exchange (see, e.g., Ref. [12]).

The presence of a long-lived primordial χ^* component can also lead to signals in terrestrial direct detection experiments. In particular, if χ^* makes up a subcomponent of the galaxy's DM halo, down-scattering off of electrons $\chi^*e \rightarrow \chi e$ leads to a mono-energetic recoil energy of approximately $E_R \simeq \mu \delta/m_e$ (provided that the mass splitting is greater than $\delta \gtrsim \mu v^2$) where v is the χ^* velocity. In the limit that $\delta \ll m_\chi \ll m_{A'}$, the differential cross section for down-scattering is

$$\frac{d\sigma}{dE_R} \simeq \frac{8\pi \alpha \alpha_D \epsilon^2 m_e}{m_{A'}^4 v^2} . \quad (3.8)$$

At the level of our “free” electron approximation, the expected signal rate R is then given by

$$R \equiv \frac{dN_{\text{sig}}}{dt dM_{\text{det}}} \simeq \text{effic.} \times \frac{N_A Z_{\text{free}}}{A g} \frac{f_* \rho_\chi}{m_\chi} \frac{8\pi \alpha \alpha_D \epsilon^2 m_e}{m_{A'}^4} \int_0^\infty dE_R \int_{v_{\min}}^\infty dv \frac{f_{\text{halo}}(v)}{v} , \quad (3.9)$$

where “effic.” accounts for the detector efficiency, $\rho_\chi \simeq 0.4 \text{ GeV}/\text{cm}^3$ is the local DM energy density, $v_{\min} \simeq |m_e E_R - \mu \delta|/(\mu \sqrt{2m_e E_R})$ is the minimum kinematically allowed χ^* velocity, M_{det} is the detector mass, N_A is Avogadro's number, Z_{free} is the number of electrons in the $n = 3, 4$ orbitals of xenon, and A is the atomic mass. Approximating the halo velocity distribution $f(v)$ as Maxwellian with dispersion $v_0 \ll \sqrt{\delta/\mu}$, the recoil energy and velocity integrals reduce to

$$\int_0^\infty dE_R \int_{v_{\min}}^\infty dv \frac{f_{\text{halo}}(v)}{v} \simeq \frac{(2\mu)^{3/2} \delta^{1/2}}{m_e} . \quad (3.10)$$

Using this in Eq (3.9) then leads to

$$R \sim 10^6 \text{ (tonne-year)}^{-1} \times f_* \left(\frac{\delta}{\text{keV}} \right)^{1/2} \left(\frac{y}{10^{-10}} \right) \left(\frac{m_\chi}{100 \text{ MeV}} \right)^{-5} . \quad (3.11)$$

Hence, even a very subdominant primordial fraction $f_* \ll 1$ may potentially lead to detectable rates.

In Figs. 2 and 3, we highlight regions of parameter space in which an excited component of the DM energy density leads to electron down-scattering event rates at XENON1T, ranging from $(1 - 100)/(\text{tonne-year})$. As shown in Fig. 1, larger α_D leads to a smaller primordial χ^* abundance, thus suppressing the down-scattering rate in terrestrial detectors. Also shown are regions excluded from recent missing energy/momentum searches at the low-energy accelerator experiments NA64 and BaBar [43, 44], as well as the projected sensitivities of a search for similar signals at LDMX and Belle II [45–48].

Fig. 2 focuses on the $\epsilon - m_\chi$ parameter space. In a standard cosmology, χ freezes out via $\chi\chi^* \leftrightarrow ff$ with an abundance consistent with the observed DM energy density along the black contours. Above or below these contours, χ is a subdominant DM component or is overabundant assuming a standard cosmology. For concreteness, when calculating the signal even rate we take χ to make up all of the DM throughout all of the parameter space shown. In Fig. 3, ϵ is varied consistently in the $\alpha_D - m_\chi$ plane such that χ makes up all of the DM energy density. Regions in excess of 100/tonne-year are constrained by a recently reported search for electron recoils in XENON1T [30].

Assuming that thermal decoupling of $\chi\chi^* \leftrightarrow ff$ sets the late-time χ abundance, scenarios in which the ground state χ makes up a subdominant component of the DM lead to increasingly larger signal rates for χ^* down-scattering in terrestrial detectors. To see this, note that if $\chi\chi^* \leftrightarrow ff$ decouples at temperatures much greater than δ , then $f_\chi \propto 1/(\alpha_D \epsilon^2)$, where $f_\chi \equiv n_\chi/n_{\text{DM}} \leq 1$ is the DM fraction composed of χ . If the decoupling of $\chi^*\chi^* \leftrightarrow \chi\chi$ is responsible for setting the χ^* abundance at much later times, then $f_* \propto 1/(\alpha_D^2 f_\chi)$. The down-scattering signal rate at direct detection experiments is then controlled by the product $f_* f_\chi \alpha_D \epsilon^2 \propto f_* \propto 1/(\alpha_D^2 f_\chi)$. Hence, smaller χ abundances imply larger signals in such cosmologies.

4 Excited States from the Sun

When the excited state χ^* is no longer stable due to the existence of, e.g., an electromagnetic dipole transition, the primordial abundance of χ^* can be severely depleted if the decay lifetime is much shorter than the age of the universe. In this case, the production and successful detection of χ^* at direct detection experiments are only possible with a source of up-scattering.

For a decay lifetime that is much larger than 1 AU divided by dark matter velocity, the Sun can act as a source of χ^* . The Sun has a high internal temperature which we take to be $T_\odot = 1.1 \text{ keV}$, and is capable of up-scattering the DM particles that come through it with $\sim \text{keV}$ energies. Gravitational focusing due to the large gravitational field also enhances the flux of DM particles incident on the solar core.

The idea to use “reflected” DM from the Sun was proposed in Ref. [49] in the context of elastic scattering. However, typically the reflected rates and energies are sufficiently low that the terrestrial experiments are typically more sensitive to the background primordial flux. This is not the case for inelastic WIMPs. For light WIMPs, even $\delta \sim 100 \text{ eV}$ can be inaccessible for up-scattering in a terrestrial experiment from the standard DM flux. Thus,

any production in the sun of an excited state which is suitably long-lived can produce a signal in a terrestrial experiment which would otherwise be absent.

To calculate the rate, we consider the problem as follows. Infalling DM particles in the core of the Sun have velocities $v \sim v_{\text{esc}} = 5 \times 10^{-3} c = 1500 \text{ km sec}^{-1}$, the escape velocity at the surface of the core. This is a high velocity compared to typical halo DM, $v_0 \sim 10^{-3} c$. However, the electrons in the sun are moving with velocity $v_e \sim \sqrt{2T/m_e} \sim 0.05 c = 1.5 \times 10^4 \text{ km sec}^{-1}$. Since $v_{\text{esc}} \ll v_e$, we should think about the solar up-scattering with DM particles being essentially at rest, and being bombarded by thermal electrons from all around them. The quantity of interest is therefore the steady-state density of DM in the sun, and not the flux of DM on the sun.

The number density $n_{\chi,\odot}$ of χ in the core of the sun is simple to determine. Infalling DM is gravitationally focused, enhancing the solar cross section by a factor $1 + v_{\text{esc}}^2/v_0^2$. Inside the sun, this appears as an enhancement of the overall DM number density. On the other hand, the higher velocity spreads the DM particles more thinly due to conservation of flux, suppressing the density by v_{esc}/v_0 . Thus, we have $n_{\chi,\odot} \simeq n_0 \times v_{\text{esc}}/v_0$.¹ The flux Φ of χ^* on Earth is then given by

$$\Phi = n_e \langle \sigma_{\chi \rightarrow \chi^*} v_e \rangle \times \frac{n_{\chi,\odot} V_\odot}{4\pi(1 \text{ AU})^2}, \quad (4.1)$$

where $\langle \sigma_{\chi \rightarrow \chi^*} v_e \rangle$ is the velocity-averaged cross-section of $\chi e^- \rightarrow \chi^* e^-$, and V_\odot is the volume of the sun's core. We also have the derivative of the flux with respect to kinetic energy K_{χ^*} of the up-scattered χ^* , written explicitly as

$$\frac{d\Phi}{dK_{\chi^*}} = n_e \left\langle \frac{d\sigma_{\chi \rightarrow \chi^*}}{dK_{\chi^*}} v_e \right\rangle \times \frac{n_{\chi,\odot} V_\odot}{4\pi(1 \text{ AU})^2}. \quad (4.2)$$

We take the solar parameters to be $V_\odot = 2.2 \times 10^{31} \text{ cm}^3$ and $n_e = 2 \times 10^{25} \text{ cm}^{-3}$ which is approximately the mean electron density in the solar core [50]. To get a sense of how large this flux is, We can compare this to the background flux of DM particles in the halo, $\Phi_0 = n_0 v_0$:

$$\begin{aligned} \frac{\Phi}{\Phi_0} \simeq 5 \times 10^{-8} & \left(\frac{n_e}{2 \times 10^{25} \text{ cm}^{-3}} \right) \left(\frac{220 \text{ km/s}}{v_0} \right) \\ & \times \left(\frac{\langle \sigma_{\chi \rightarrow \chi^*} v_e \rangle}{10^{-30} \text{ cm}^3 \text{ s}^{-1}} \right) \left(\frac{V_\odot}{2.2 \times 10^{31} \text{ cm}^3} \right) \left(\frac{v_{\text{esc}}/v_0}{7.0} \right). \end{aligned} \quad (4.3)$$

A simple expression for $\langle \sigma_{\chi \rightarrow \chi^*} v_e \rangle$ can be found in the nonrelativistic limit and with $\delta \ll m_e, m_\chi$, since the electron velocity distribution is Maxwellian. The differential scattering cross section in this limit is

$$\frac{d\sigma_{\chi \rightarrow \chi^*}}{dK_{\chi^*}} = \frac{\bar{\sigma}_e m_\chi}{2\mu_{\chi e}^2 v_e^2}, \quad (4.4)$$

¹Precisely, the focusing is true for a $1/r$ potential. Inside the sun, this is no longer the case. However, approximately 50% of the mass of the Sun is contained inside of $r < r_\odot/4$. Thus, we consider the $1/r$ potential to be reasonable down to these distances at the level of accuracy we have here.

where K_χ is the recoil kinetic energy of χ , and $\bar{\sigma}_e$ is defined in Eq. (2.2). The velocity-averaged cross section is then

$$\langle \sigma_{\chi \rightarrow \chi^* v_e} \rangle = \int_0^\infty dK_{\chi^*} \int_{v_{\min}}^\infty dv_e f_{\text{MB}}(v_e) \frac{d\sigma}{dK_{\chi^*}} v_e, \quad (4.5)$$

where v_{\min} is the minimum velocity at fixed K_χ given by the kinematics of the up-scattering,

$$v_{\min} = \frac{1}{\sqrt{2m_\chi K_{\chi^*}}} \left(\frac{m_\chi K_{\chi^*}}{\mu_{\chi e}} + \delta \right), \quad (4.6)$$

and $f_{\text{MB}}(v_e)$ is the Maxwell-Boltzmann velocity distribution,

$$f_{\text{MB}}(v_e) = 4\pi v_e^2 \left(\frac{m_e}{2\pi T_\odot} \right)^{3/2} \exp \left(-\frac{m_e v_e^2}{2T_\odot} \right). \quad (4.7)$$

The integrals in Eq. (4.5) can be evaluated analytically, giving

$$\langle \sigma_{\chi \rightarrow \chi^* v_e} \rangle = \bar{\sigma}_e \sqrt{\frac{2m_e}{\pi T_\odot}} \frac{\delta}{\mu_{\chi e}} \exp \left(-\frac{m_e \delta}{\mu_{\chi e} T_\odot} \right) K_1 \left(\frac{m_e \delta}{\mu_{\chi e} T_\odot} \right) \quad (4.8)$$

$$\simeq \bar{\sigma}_e \begin{cases} \sqrt{\frac{2T_\odot}{\pi m_e}}, & 2\delta/\mu_{\chi e} \ll 2T_\odot/m_e, \\ \sqrt{\frac{2\delta}{\mu_{\chi e}}} \exp \left(-\frac{m_e \delta}{\mu_{\chi e} T_\odot} \right), & 2\delta/\mu_{\chi e} \gg 2T_\odot/m_e, \end{cases} \quad (4.9)$$

where we have expanded the Bessel function K_1 assuming a large argument for the final approximation. The factor of $\sqrt{2\delta/\mu_{\chi e}}$ is a characteristic velocity of the up- and down-scattering process, with the exponential suppression coming from the fact that only electrons with $v_e \gtrsim \sqrt{2\delta/\mu_{\chi e}}$ are capable of up-scattering χ . Consequently, the cross section is not suppressed exponentially compared to the elastic cross section if $\delta \sim T_\odot$. However, we still have a somewhat surprising fact in that inelasticity benefits the signal tremendously. Ordinarily, the DM can only carry away $\sim \mu^2/m_\chi m_e \sim m_e/m_\chi$ fraction of the energy. However, because of the inelasticity, χ 's can exit the sun with a substantial amount of energy to deposit in the detector. Thus, although the scattering rate is not significantly changed from the elastic case, the *detectable* signal has been enhanced tremendously.

While primordial down-scatters yield a narrow recoil electron spectrum in direct detection experiments centered on the splitting δ , the χ^* flux from the sun is broadened by the scattering off the thermal distribution of electrons; the rate per energy of χ^* particles produced for $m_\chi = 3.7$ MeV thermal DM with a splitting of $\delta = 3.5$ keV is shown in Fig. 4.

With the DM flux per energy $d\Phi/dK_{\chi^*}$ in Eq. (4.2), we can write the electron recoil spectrum per detector mass per time dR/dE_R observed at a direct detection experiment as

$$\frac{dR}{dE_R} = \frac{N_T}{M_{\text{det}}} \int dK_{\chi^*} \frac{d\Phi}{dK_{\chi^*}} \frac{d\sigma_{\chi^* \rightarrow \chi}}{dE_R}, \quad (4.10)$$

where E_R is the electron recoil energy, $\sigma_{\chi^* \rightarrow \chi}$ is the down-scattering cross section, N_T is the number of targets in the detector, and M_{det} is the detector mass. This expression can be

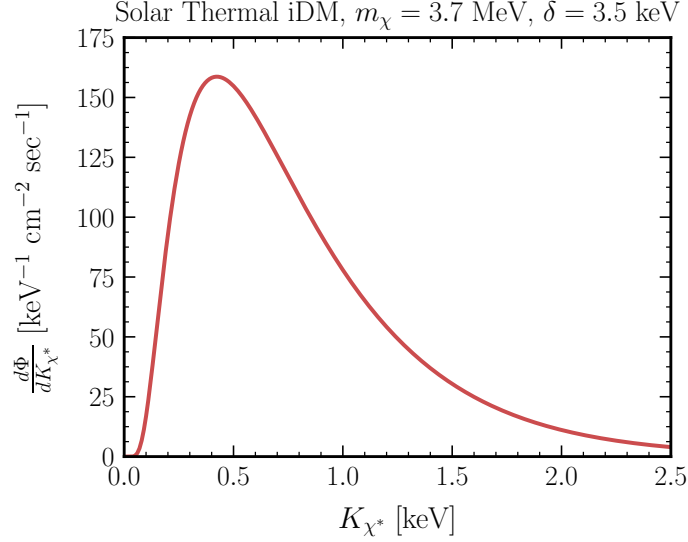


Figure 4: The flux Φ of χ^* particles up-scattered by electrons per energy K , assuming $m_\chi = 4 \text{ MeV}$, $\delta = 3.5 \text{ keV}$ and a thermal annihilation cross section.

evaluated numerically, but we can gain significant analytic understanding of R , the expected number of events per detector mass per time, at a direct detection experiment by assuming the nonrelativistic limit and $\delta \ll m_e, m_\chi$ once again. In this limit, the down-scattering cross section can be written in a particularly simple form:

$$\frac{d\sigma_{\chi^* \rightarrow \chi}}{dE_R} \simeq \frac{\bar{\sigma}_e m_e}{2\mu_{\chi e}^2 v_{\chi^*}^2}. \quad (4.11)$$

The cross section of scattering for a given DM velocity v_{χ^*} can be obtained by integrating this expression up to the kinematic limit. In the elastic limit, this simply gives $\bar{\sigma}_e$; however, the existence of the splitting δ can extend this kinematic limit significantly, giving $\sigma_{\chi^* \rightarrow \chi} \simeq F \bar{\sigma}_e$, where following Eq. (2.5) we have

$$F \equiv \sqrt{1 + \frac{2\delta}{\mu_{\chi e} \langle v_{\chi^*}^2 \rangle}}, \quad (4.12)$$

with $\langle v_{\chi^*}^2 \rangle$ the mean square velocity of χ^* from the sun; examining the kinematics of the χ -electron scattering shows that

$$\langle v_{\chi^*}^2 \rangle = \frac{8\mu_{\chi e}^2 T_\odot}{m_\chi^2 m_e}. \quad (4.13)$$

F represents an enhancement with respect to the elastic scattering cross section, which is significant whenever the velocity scale $2\delta/\mu_{\chi e} \gg v_{\chi^*}^2$. With this result, we can write R as

$$R \simeq \frac{N_T}{M_{\text{det}}} \Phi F \bar{\sigma}_e. \quad (4.14)$$

Combining the equation with the expression for the ratio of the solar flux to the DM halo flux in Eq. (4.3) and the analytic estimate for $\langle\sigma_{\chi\rightarrow\chi^*v_e}\rangle$ in Eq. (4.9), we obtain the following numerical estimate for R for a xenon experiment in the solar inelastic DM model:

$$R \simeq 23 \text{ (tonne-year)}^{-1} \left(\frac{n_e}{2 \times 10^{25} \text{ cm}^{-3}} \right) \left(\frac{\bar{\sigma}_e}{10^{-38} \text{ cm}^2} \right)^2 \left(\frac{V_\odot}{2.2 \times 10^{31} \text{ cm}^3} \right) \left(\frac{v_{\text{esc}}/v_0}{7.0} \right) \\ \times \left(\frac{\rho_0}{0.3 \text{ GeV cm}^{-3}} \right) \left(\frac{4 \text{ MeV}}{m_\chi} \right) \left(\frac{F}{8.0} \right) \left(\frac{\sqrt{2\delta/\mu_{\chi e}} \exp[-m_e\delta/\mu_{\chi e}T_\odot]}{3 \times 10^{-3}} \right), \quad (4.15)$$

where ρ_0 is the local DM mass density. The values shown for comparison are either exactly the solar parameters adopted for our calculations, or are close to the actual values of these parameters when $m_\chi = 4 \text{ MeV}$.

Armed with this analytic understanding, we are now ready to examine the numerical results. In Fig. 5, we show an expected solar inelastic DM spectrum dR/dE_R at XENON1T, together with the latest measurement of the event rate in the $(0 - 30) \text{ keV}$ range and the experiment's background model [30]. Here, we have chosen parameters that are consistent with a thermal inelastic DM model, with $m_\chi = 4 \text{ MeV}$, $m_{A'}/m_\chi = 3$ and $\delta = 3.5 \text{ keV}$; these parameters lead to approximately 60 events per tonne-year at a xenon detector. Because the DM flux is generated by scattering with thermal electrons in the solar core, the expected spectrum detected is significantly broader than the line-like signal expected from the primordial model.

Fig. 6 (left) shows the expected rate R at XENON1T as a function of the DM mass m_χ and the splitting δ . For small splittings $\delta \ll T_\odot$, the enhancement in the down-scattering rate encoded in F is close to 1, leading to a small rate. As the splitting increases to $\delta \sim \text{keV}$, the enhancement becomes significant, and event rates of 100 per tonne-year can be expected for $m_\chi \lesssim 5 \text{ MeV}$. Once $\delta \gg T_\odot$, however, few electrons in the solar core have sufficient energies to up-scatter χ , leading to the exponential suppression shown in Eq. (4.15). For a thermal model, since $\bar{\sigma}_e \propto \langle\sigma v\rangle_{\text{ann}} \mu_{\chi e}^2/m_\chi^2$ and for a sufficiently large splitting, $F \propto m_\chi$, we obtain $R \propto \delta e^{-m_e\delta/(\mu_{\chi e}T_\odot)} m_\chi^{-4}$, leading to a power law drop in R as m_χ increases, and an exponential decrease as δ increases. There are currently no other experimental constraints in this range of parameters, but LDMX [47, 48] will be sensitive to this entire space.

Fig. 6 (right) shows a similar result but in the m_χ - f_χ plane, where f_χ is the fractional mass abundance of χ , which we assume to be thermally produced. Under this assumption, $\rho_\chi \propto f_\chi$ and $\langle\sigma v\rangle \propto 1/f_\chi$, and so the overall rate at a direct detection experiment grows as $1/f_\chi$, making subdominant components easier to detect. A similar argument as before gives $R \propto f_\chi^{-1} m_\chi^{-4}$, so that lines of constant event rate on the m_χ - f_χ plane follows $f_\chi \propto m_\chi^{-4}$. XENON1T can probe thermal iDM through solar scattering of all abundances below 10 MeV for $\delta \sim 3 \text{ keV}$. Other constraints on this plane include the NA64 experiment [43], which has ruled out all sub-100 MeV thermal dark matter with $f_\chi \lesssim 0.01$, and the future LDMX experiment [47, 48] which probes a similar parameter space to XENON1T.

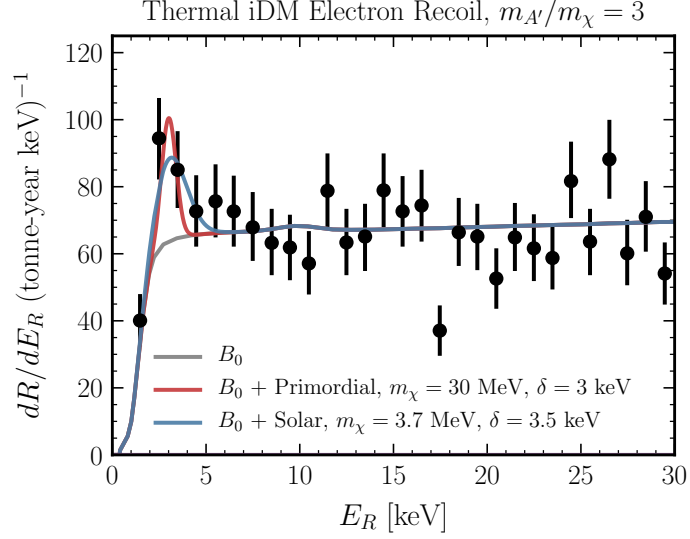


Figure 5: Detected electron recoil spectrum in the XENON1T experiment. We show the background model B_0 (gray) provided by Ref. [30], together with the B_0 +signal for the thermal inelastic DM in the solar up-scattering with $m_\chi = 3.7$ MeV, $\delta = 3.5$ keV (blue) and the primordial excited states scenarios with $m_\chi = 30$ MeV, $\delta = 3$ keV (red).

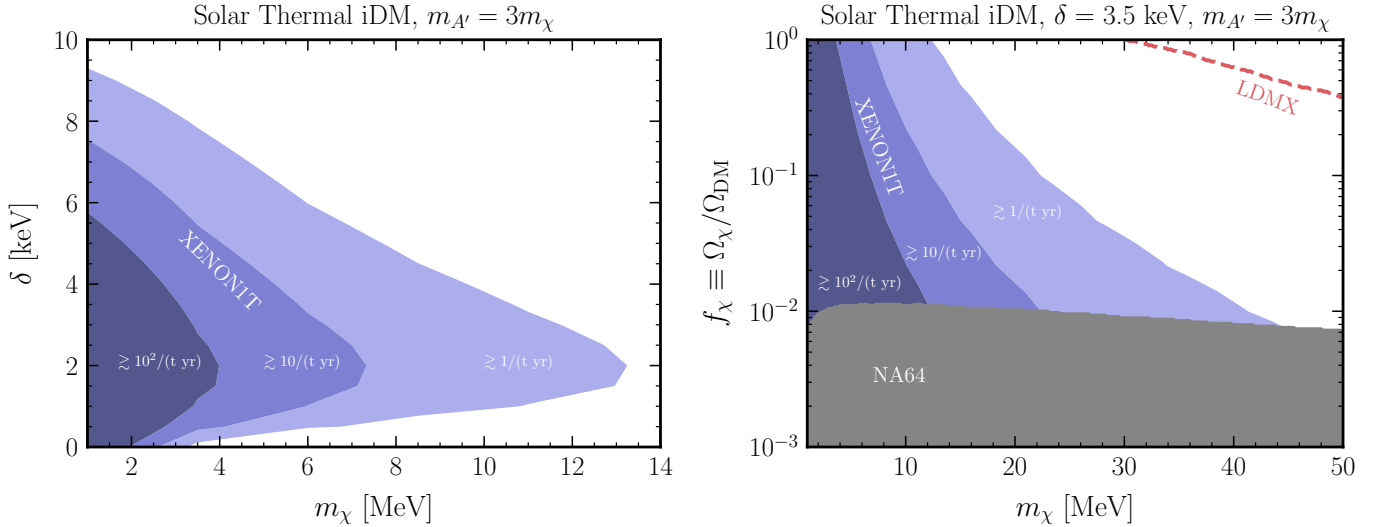


Figure 6: (Left) Expected event rate at XENON1T for the solar thermal inelastic DM model (blue), as a function of DM mass m_χ and the splitting δ (left) and as a function of m_χ and the thermal DM abundance by mass f_χ (right). Current limits from NA64 [43] (gray) as well as the future reach of LDMX [47, 48] (red, dashed) are also shown. Note that the entire m_χ - δ parameter space will be probed by LDMX.

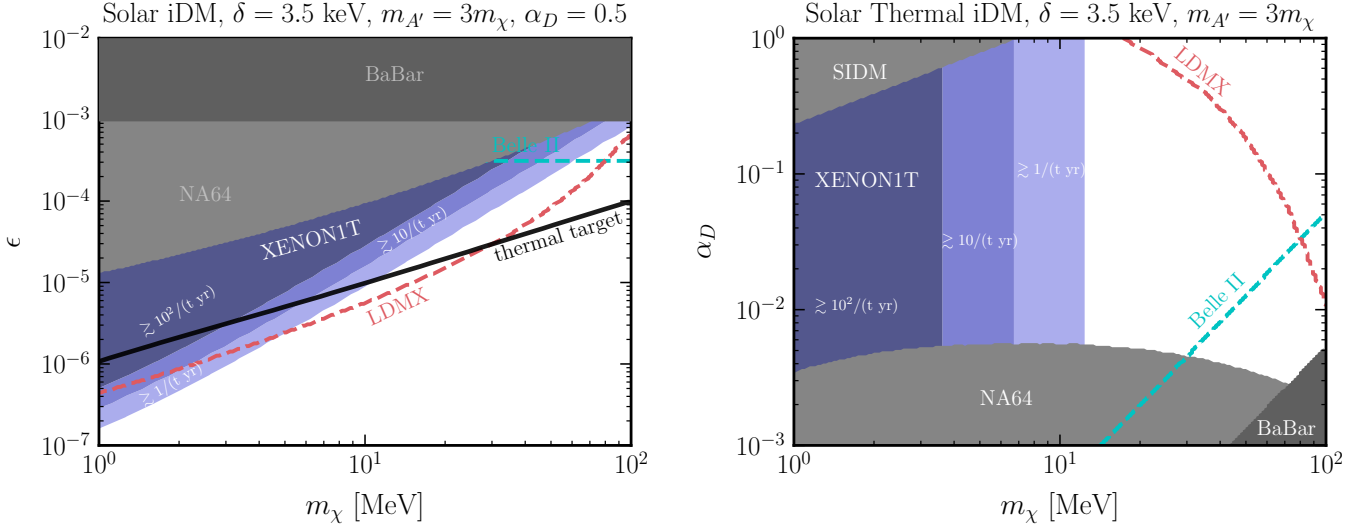


Figure 7: (Left) Expected event rate at XENON1T for the solar inelastic DM model (blue), as a function of m_χ and ϵ *without* assuming thermal production (left), and as a function of m_χ and α_D *with* thermal production. Current constraints from NA64 [43], BaBar [44] and self-interaction of DM [41] are shown in gray, with the future reaches of Belle II [10, 46] (green, dashed) and LDMX [47, 48] (red, dashed) displayed in both plots.

In Fig. 7 (right), we consider the m_χ - α_D plane for a thermally produced dark matter with $f_\chi = 1$. In this plane, the rate does not depend on α since ϵ is always chosen to hold $\langle\sigma v\rangle_{\text{ann}}$ approximately constant. Once again, we see the relation $R \propto m_\chi^{-4}$. At higher DM masses $m_\chi \gtrsim 30$ MeV, current and future B -factories like BaBar [44] and Belle II [10, 46]. Self-interaction limits of $10 \text{ cm}^2 \text{ g}^{-1}$ [41] also place constraints at large values of α_D and small values of m_χ .

Finally, in Fig. 7 (left), we lift the assumption of a thermally produced dark matter, but still assume that χ makes up all of the dark matter through some nonthermal production mechanism that we do not specify. After fixing the coupling $\alpha_D = 0.5$, the mixing parameter ϵ is still a free parameter; we show the region of parameter space where we expect 1–100 events per tonne-year in XENON1T, as well as existing and future beam dump constraints. Without the thermal dark matter assumption, the choice of $m_{A'}/m_\chi = 3$ means that $\bar{\sigma}_e \propto m_\chi^{-8}$, so that overall the event rate at XENON1T scales as $R \propto \epsilon^4 m_\chi^{-8}$. For this particular choice of mass splittings, we can see that xenon direct detection experiments have the potential to probe the thermal target line up to $m_\chi \sim 20$ MeV, with a reach comparable to that of the future LDMX.

Note that constraints from indirect detection and the CMB power spectrum do not apply to the solar inelastic DM, since we assume that the excited state is completely depleted over cosmological timescales, making the annihilation of χ_1 into Standard Model particles

negligible.

It has been argued that there are signs of astrophysical excesses in X-ray spectra at 3.5 keV [51, 52]. DM up-scattering followed by a decay through a dipole has been proposed as an explanation [53, 54]. It was argued that a very large dipole couple mediate electron-DM scattering in hot gas, yielding an excited state [54]. Here, we revisit the idea of excitation, but mediated by the dark photon interaction.

In Ref. [54] it is claimed that the rate from the Perseus cluster from DM excitation can be computed to be

$$\Phi \simeq 10^{-5} \text{ sec}^{-1} \text{ cm}^{-2} \times \left(\frac{\text{MeV}}{m_\chi} \right) \left(\frac{\langle \sigma v \rangle}{10^{-24} \text{ cm}^3 \text{ sec}^{-1}} \right). \quad (4.16)$$

This should be compared to the flux from Perseus of around $10^{-5} \text{ sec}^{-1} \text{ cm}^{-2}$. A similar calculation to that of the sun, but using $T = 6.8 \text{ keV}$ yields $\langle \sigma v \rangle \simeq 4 \times 10^{-29} \text{ cm}^3 \text{ sec}^{-1}$ for $m_\chi = 4 \text{ MeV}$ and $\delta = 3.5 \text{ keV}$, several orders too low the putative signal. Moreover, if it is thermal, increasing the cross section will decrease the relic abundance, so the expected rate is the same, even for a subdominant component of DM. Nonetheless, the possibility is intriguing and we leave a detailed study for future work.

5 Excited States from the Earth

Finally, we consider excited states with the shortest lifetimes, which can be populated locally by dark-photon-mediated up-scattering in the Earth. Subsequent electromagnetic decays can yield a detectable signal in parts of parameter space where the scattering process itself is currently unobservable. These classes of ‘luminous’ models have been considered in the context of dipole up-scattering in the Earth [8, 55], in material near the target [56], or even in the detector itself [7, 57].

Unlike in the hot environments in the Sun and the early universe, the relative velocities on Earth are too low for DM-electron scattering to populate splittings on the scale of a keV, so we focus here on nuclear scatterings. Furthermore, the DM must have sufficient mass to kinematically up-scatter at velocities $\sim 10^{-3} c$: for $\delta \sim \text{keV}$ one must have $m_\chi \gtrsim \text{GeV}$ to scatter without kinematical suppression. At the same time, for $m_\chi \gtrsim 10 \text{ GeV}$, the energy deposited in the detector directly through nuclear recoil can become observable. Thus the range of primary interest for up-scattering followed by electromagnetic de-excitation in the models we are considering is $m_\chi \sim \mathcal{O}(\text{GeV})$.

In this mass range, the thermal relic makes up the full DM abundance for $y \sim 10^{-8}$, with a DM-proton scattering cross section of $\sigma_p \simeq 2 \times 10^{-37} \text{ cm}^2 \left(\frac{\text{GeV}}{m_\chi} \right)^2$ in the elastic limit. While the elastic cross section of this magnitude is excluded by CRESST [58], a splitting δ produces a kinematic suppression f_{inel} in the scattering rate of $f_{\text{inel}} \sim 10^{-2} - 10^{-5}$ for $\text{keV} \lesssim \delta \lesssim 2 \text{ keV}$ at $m_\chi \simeq \text{GeV}$, and $f_{\text{inel}} \sim 10^{-1} - 10^{-7}$ for $\text{keV} \lesssim \delta \lesssim 2.5 \text{ keV}$ at $m_\chi \simeq 1.2 \text{ GeV}$, with steep sensitivity to the masses and halo parameters. This suppression is important because it also naturally suppressed signals in nuclear recoils in direct detection experiment. For

$f_{\text{inel}}\sigma_p \sim 10^{-42}\text{cm}^2$, for instance, particles of $m_\chi = 3\text{ GeV}$ would evade current limits. Without the inelastic suppression they would already have been excluded.

Each volume unit in the Earth acts as a source of up-scattered states and generates a local flux at a detector. Considering the Earth as composed of crust, mantle and core, and the scatterings dominated by silicon and iron densities as in Ref. [55], we find the resulting flux of up-scattered excited states relative to the DM flux is given by

$$\Phi_*/\Phi_{\text{DM}} \sim \frac{f_{\text{inel}}\sigma_p}{5 \times 10^{-34}\text{cm}^2}, \quad (5.1)$$

At splittings close to the kinematic threshold, the flux is further enhanced because the up-scattered states have lower average velocity than that of the DM.

Because the cross sections are proportional to the reduced mass of the system, the electron down-scattering cross section is suppressed by a factor $\sim m_e^2/m_\chi^2 \sim 10^{-6}$. However, for lifetimes long compared to the time to traverse the Earth R_E/v , the decays can produce significant event rates in direct detection experiments. As previously discussed, a lifetime of 100 sec requires a dipole suppressed $\Lambda_d \gtrsim 100\text{TeV}$.

The rate per unit mass in XENON1T is approximately,

$$R \sim \frac{60}{\text{tonne} - \text{year}} \left(\frac{f_{\text{inel}}}{10^{-5}} \right) \left(\frac{\sigma_p}{10^{-37}\text{cm}^2} \right) \left(\frac{\text{GeV}}{m_\chi} \right) \left(\frac{100\text{sec}}{\tau} \right) \quad (5.2)$$

Here, the lifetime of 100 seconds allows the entire Earth to act as a source.

While the inelastic suppression and unknown lifetime makes quantitative expectations very challenging, it is still noteworthy that a thermal relic can naturally give a detectable rate in the GeV mass range. Moreover, as before, if this is a subdominant component, the increased cross section and decreased abundance will cancel, leaving the overall rate intact. We thus conclude that a thermal relic is quite capable of yielding a photon signal in direct detection experiments, although with no real handle on the precise rate.

The excited states propagate outside the Earth and can decay outside, producing a diffuse X-ray background peaked at the energy of the splitting. As the states are generated in the Earth, the flux of decaying state falls off as $1/r^2$ and the X-ray signal is dominated by the excited DM particles closest to the Earth. The rate is directly proportional to the volumetric rate $dN/dtdV$ in a DM direct detection experiment, yielding a flux of

$$\Phi_{\text{diffuse}} \sim 0.1 \frac{\text{photons}}{\text{sr cm}^2 \text{sec}} \left(\frac{dN/dtdV}{10^4 \text{ m}^3 \text{ year}} \right) \quad (5.3)$$

The limits are $O(0.1) \text{ sr}^{-1} \text{ cm}^{-2} \text{ sec}^{-1}$ in this energy range [59], making current terrestrial detectors more sensitive than X-ray satellites, as long as the decay length is large compared to the Earth radius.

In addition, DM-DM scattering can give rise to a population of excited states which then decay, again giving rise to a potential excesses in X-ray spectra [53], with flux comparable to the flux of Perseus for large enough cross sections,

$$\Phi_{\text{Perseus}} \simeq 10^{-5} \text{ sec}^{-1} \text{ cm}^{-2} \times \left(\frac{\text{GeV}}{m_\chi} \right)^2 \left(\frac{\langle \sigma v \rangle}{10^{-21} \text{ cm}^3 \text{ sec}^{-1}} \right). \quad (5.4)$$

For GeV-mass DM considered here, we find $\langle\sigma v\rangle\sim 10^{-21}\text{ cm}^3\text{ sec}^{-1}$, potentially of the right order to source the tentative signal.

6 Discussion

Models of light dark matter are simple and viable and result in a new class of experimental signatures. For light fermions coupled to a dark photon, CMB constraints naturally point to a pseudo-Dirac class of models. These models come with an excited state that is often swept aside in the discussion of the DM phenomenology. In this paper, we have considered these excited states and their implications. We have found that far from being a side note, these excited states can offer powerful signatures of this class of DM models. The fact that the scenarios we have considered may explain the putative excess at XENON1T adds to the excitement.

We have investigated three separate scenarios: primordial excitations, excitations in the sun, and excitations in the Earth. Each of them probes different regions of parameter space, and provides different implications for future data and experiments.

For primordial excitations, we have found that the abundance of the excited state typically becomes exponentially suppressed, with excited fractions as small as $f_*\sim 10^{-9}$ arising for light thermal dark matter. We find this is true for splittings over a wide range of $\sim\text{keV}-100\text{ keV}$. Larger $m_\chi\sim\text{GeV}$ mass particles see less pronounced, but still present, suppression of the excited state abundance. Note that this is quite unlike previous scenarios with heavy DM particles, where often χ and χ^* are present in roughly equal abundances.

The suppression of the excited state abundance naturally changes the signal rate. Nonetheless, we find that existing and upcoming liquid Xenon experiments exclude some regions of parameter space for light dark matter, and are sensitive to much of the remainder. In particular, we find that for thermal relic DM and low values of α_D , these scenarios predict in excess of 100 events/tonne/year at a Xenon experiment. For larger values of α_D , lower rates are possible, but still in excess of 1 event/tonne/year is expected, making future Xenon experiments capable of testing much of this remaining parameter space. Much, but not all, of the parameter space will be tested by LDMX and Belle II as well. Remarkably, subdominant components are even *more* constrained by experimental searches as they typically have a higher rate of primordial fraction. A signal here would show as a fairly narrow line.

For cases where the primordial states are unstable, this will not be a signal. However, local up-scatterings offer promise over a narrow, yet interesting, parameter space.

The Sun is capable of up-scattering light dark matter into the excited state in cases where $\delta\sim T_\odot$. This allows dark matter to carry energy out of the sun and then deposit it into terrestrial experiments at energies above threshold. For a thermal relic making up all of the dark matter, one can expect detectable rates up to splittings as large as 10 keV and masses up to 13 MeV. For subdominant components, the scattering rate in the sun remains constant as the parameters of the theory are increased, thus the flux of excited states at Earth does not decrease even for subdominant components of dark matter (until the Sun becomes

opaque to them). However, the scattering cross section goes up and thus again we find direct detection experiments are more sensitive to subdominant components of dark matter, i.e., when $\rho_\chi < \rho_{\text{DM}}$. We find interesting signal rates up to masses of ~ 50 MeV. This entire parameter space should be tested by LDMX.

An important difference between these two cases is that solar scatters naturally have a measurable line width. With sufficient data, this should be a means of distinguishing these two cases.

For \sim GeV masses, DM can up-scatter via the dark photon in the Earth. These up-scatters can then decay via photon emission as in the Luminous Dark Matter proposal. There is a narrow window at the GeV scale where one can up-scatter at a detectable rate without conflicting with existing nuclear recoil experiments. Such a rate would likely be detectable by future X-ray satellites.

Given the recent claim of an excess of electron events at XENON1T, it is exciting to consider these three scenarios as possible sources. From our results, we believe all three scenarios are capable of producing an excess. All three make concrete predictions for future experiments. Future datasets from liquid Xenon experiments will be able to differentiate the energy spectra of the line shape predicted by the primordial abundance and the Earth up-scattering scenario versus the broader signal expected from solar up-scattering.

All three scenarios require an excited state near 3.5 keV to explain the XENON1T data. Intriguingly, there have been claims of excess X-ray emission from a variety of astrophysical sources in that range. It is interesting to consider if these could be related.

For up-scatters in the Earth from a dark photon, the natural size of the cross section is adequate to explain the Perseus excess. For the lighter, solar up-scattered model, the rate is far short of what is needed. Nonetheless, it remains an intriguing possibility. Conversely, some models that might explain the 3.5 keV line can be constrained by our analyses here.

In summary, we have considered the electromagnetic signals arising from the excited states that are almost inevitable in models of light fermionic dark matter. We find the presence of these excited states leads to signals which already today constrain the parameter space and provides exciting possibilities for discovery in the future. Any signal from these models are testable in the future, by direct detection and experiments such as LDMX. With adequate data, the solar up-scatter scenario can be distinguished by spectrum alone.

Acknowledgments

We thank Rouven Essig for being Rouven Essig and Ken Van Tilburg for helpful discussions and comments on the manuscript. We are also grateful to Natalia Toro for discussions and insight arising from not-yet published work. AB and MB are supported by the James Arthur Fellowship. HL is supported by the DOE under contract DESC0007968 and the NSF under award PHY-1915409. NW is supported by NSF under award PHY-1915409 and the Simons Foundation. This research made use of the IPython [60], Jupyter [61], matplotlib [62], NumPy [63], seaborn [64], SciPy [65], and tqdm [66] software packages.

References

- [1] D. Tucker-Smith and N. Weiner, *Inelastic dark matter*, *Phys. Rev. D* **64** (2001) 043502 [[hep-ph/0101138](#)].
- [2] D. P. Finkbeiner, T. R. Slatyer, N. Weiner and I. Yavin, *PAMELA, DAMA, INTEGRAL and Signatures of Metastable Excited WIMPs*, *JCAP* **09** (2009) 037 [[0903.1037](#)].
- [3] B. Batell, M. Pospelov and A. Ritz, *Direct Detection of Multi-component Secluded WIMPs*, *Phys. Rev. D* **79** (2009) 115019 [[0903.3396](#)].
- [4] R. F. Lang and N. Weiner, *Peaked Signals from Dark Matter Velocity Structures in Direct Detection Experiments*, *JCAP* **06** (2010) 032 [[1003.3664](#)].
- [5] P. W. Graham, R. Harnik, S. Rajendran and P. Saraswat, *Exothermic Dark Matter*, *Phys. Rev. D* **82** (2010) 063512 [[1004.0937](#)].
- [6] D. P. Finkbeiner, T. Lin and N. Weiner, *Inelastic Dark Matter and DAMA/LIBRA: An Experimentum Crucis*, *Phys. Rev. D* **80** (2009) 115008 [[0906.0002](#)].
- [7] S. Chang, N. Weiner and I. Yavin, *Magnetic Inelastic Dark Matter*, *Phys. Rev. D* **82** (2010) 125011 [[1007.4200](#)].
- [8] B. Feldstein, P. W. Graham and S. Rajendran, *Luminous Dark Matter*, *Phys. Rev. D* **82** (2010) 075019 [[1008.1988](#)].
- [9] D. E. Morrissey and A. P. Spray, *New Limits on Light Hidden Sectors from Fixed-Target Experiments*, *JHEP* **06** (2014) 083 [[1402.4817](#)].
- [10] E. Izaguirre, G. Krnjaic and B. Shuve, *Discovering Inelastic Thermal-Relic Dark Matter at Colliders*, *Phys. Rev. D* **93** (2016) 063523 [[1508.03050](#)].
- [11] E. Izaguirre, Y. Kahn, G. Krnjaic and M. Moschella, *Testing Light Dark Matter Coannihilation With Fixed-Target Experiments*, *Phys. Rev. D* **96** (2017) 055007 [[1703.06881](#)].
- [12] A. Berlin and F. Kling, *Inelastic Dark Matter at the LHC Lifetime Frontier: ATLAS, CMS, LHCb, CODEX-b, FASER, and MATHUSLA*, *Phys. Rev. D* **99** (2019) 015021 [[1810.01879](#)].
- [13] E. Izaguirre, G. Krnjaic, P. Schuster and N. Toro, *Analyzing the Discovery Potential for Light Dark Matter*, *Phys. Rev. Lett.* **115** (2015) 251301 [[1505.00011](#)].
- [14] J. Alexander et al., *Dark Sectors 2016 Workshop: Community Report*, 8, 2016, [1608.08632](#).
- [15] N. Padmanabhan and D. P. Finkbeiner, *Detecting dark matter annihilation with CMB polarization: Signatures and experimental prospects*, *Phys. Rev. D* **72** (2005) 023508 [[astro-ph/0503486](#)].
- [16] T. R. Slatyer, N. Padmanabhan and D. P. Finkbeiner, *CMB Constraints on WIMP Annihilation: Energy Absorption During the Recombination Epoch*, *Phys. Rev. D* **80** (2009) 043526 [[0906.1197](#)].
- [17] M. S. Madhavacheril, N. Sehgal and T. R. Slatyer, *Current Dark Matter Annihilation Constraints from CMB and Low-Redshift Data*, *Phys. Rev. D* **89** (2014) 103508 [[1310.3815](#)].
- [18] P. J. Fox, G. Jung, P. Sorensen and N. Weiner, *Dark Matter in Light of the LUX Results*, *Phys. Rev. D* **89** (2014) 103526 [[1401.0216](#)].

- [19] M. T. Frandsen and I. M. Shoemaker, *Up-shot of inelastic down-scattering at CDMS-Si*, *Phys. Rev. D* **89** (2014) 051701 [[1401.0624](#)].
- [20] M. Carrillo-Gonzalez and N. Toro 2020.
- [21] R. Essig, J. Mardon and T. Volansky, *Direct Detection of Sub-GeV Dark Matter*, *Phys. Rev. D* **85** (2012) 076007 [[1108.5383](#)].
- [22] R. Essig, M. Fernandez-Serra, J. Mardon, A. Soto, T. Volansky and T.-T. Yu, *Direct Detection of sub-GeV Dark Matter with Semiconductor Targets*, *JHEP* **05** (2016) 046 [[1509.01598](#)].
- [23] R. Essig, T. Volansky and T.-T. Yu, *New Constraints and Prospects for sub-GeV Dark Matter Scattering off Electrons in Xenon*, *Phys. Rev. D* **96** (2017) 043017 [[1703.00910](#)].
- [24] SENSEI collaboration, *SENSEI: Direct-Detection Results on sub-GeV Dark Matter from a New Skipper-CCD*, [2004.11378](#).
- [25] DAMIC collaboration, *Constraints on Light Dark Matter Particles Interacting with Electrons from DAMIC at SNOLAB*, *Phys. Rev. Lett.* **123** (2019) 181802 [[1907.12628](#)].
- [26] LUX collaboration, *First Searches for Axions and Axionlike Particles with the LUX Experiment*, *Phys. Rev. Lett.* **118** (2017) 261301 [[1704.02297](#)].
- [27] PANDAX-II collaboration, *Constraining Dark Matter Models with a Light Mediator at the PandaX-II Experiment*, *Phys. Rev. Lett.* **121** (2018) 021304 [[1802.06912](#)].
- [28] XENON collaboration, *Light Dark Matter Search with Ionization Signals in XENON1T*, *Phys. Rev. Lett.* **123** (2019) 251801 [[1907.11485](#)].
- [29] PANDAX collaboration, *Limits on Axion Couplings from the First 80 Days of Data of the PandaX-II Experiment*, *Phys. Rev. Lett.* **119** (2017) 181806 [[1707.07921](#)].
- [30] XENON collaboration, *Observation of Excess Electronic Recoil Events in XENON1T*, [2006.09721](#).
- [31] B. Holdom, *Two $U(1)$'s and Epsilon Charge Shifts*, *Phys. Lett. B* **166** (1986) 196.
- [32] C. Boehm and P. Fayet, *Scalar dark matter candidates*, *Nucl. Phys. B* **683** (2004) 219 [[hep-ph/0305261](#)].
- [33] D. P. Finkbeiner and N. Weiner, *Exciting Dark Matter and the INTEGRAL/SPI 511 keV signal*, *Phys. Rev. D* **76** (2007) 083519 [[astro-ph/0702587](#)].
- [34] N. Arkani-Hamed, D. P. Finkbeiner, T. R. Slatyer and N. Weiner, *A Theory of Dark Matter*, *Phys. Rev. D* **79** (2009) 015014 [[0810.0713](#)].
- [35] M. Pospelov and A. Ritz, *Astrophysical Signatures of Secluded Dark Matter*, *Phys. Lett. B* **671** (2009) 391 [[0810.1502](#)].
- [36] D. Hooper and K. M. Zurek, *A Natural Supersymmetric Model with MeV Dark Matter*, *Phys. Rev. D* **77** (2008) 087302 [[0801.3686](#)].
- [37] S. Knapen, T. Lin and K. M. Zurek, *Light Dark Matter: Models and Constraints*, *Phys. Rev. D* **96** (2017) 115021 [[1709.07882](#)].
- [38] T. Cohen, D. J. Phalen, A. Pierce and K. M. Zurek, *Asymmetric Dark Matter from a GeV Hidden Sector*, *Phys. Rev. D* **82** (2010) 056001 [[1005.1655](#)].

- [39] R. Essig, A. Manalaysay, J. Mardon, P. Sorensen and T. Volansky, *First Direct Detection Limits on sub-GeV Dark Matter from XENON10*, *Phys. Rev. Lett.* **109** (2012) 021301 [[1206.2644](#)].
- [40] R. Catena, T. Emken, N. Spaldin and W. Tarantino, *Atomic responses to general dark matter-electron interactions*, [1912.08204](#).
- [41] S. Tulin and H.-B. Yu, *Dark Matter Self-interactions and Small Scale Structure*, *Phys. Rept.* **730** (2018) 1 [[1705.02358](#)].
- [42] PLANCK collaboration, *Planck 2018 results. VI. Cosmological parameters*, [1807.06209](#).
- [43] D. Banerjee et al., *Dark matter search in missing energy events with NA64*, *Phys. Rev. Lett.* **123** (2019) 121801 [[1906.00176](#)].
- [44] BABAR collaboration, *Search for Invisible Decays of a Dark Photon Produced in e^+e^- Collisions at BaBar*, *Phys. Rev. Lett.* **119** (2017) 131804 [[1702.03327](#)].
- [45] E. Izaguirre, G. Krnjaic, P. Schuster and N. Toro, *Testing GeV-Scale Dark Matter with Fixed-Target Missing Momentum Experiments*, *Phys. Rev. D* **91** (2015) 094026 [[1411.1404](#)].
- [46] M. Battaglieri et al., *US Cosmic Visions: New Ideas in Dark Matter 2017: Community Report*, in *U.S. Cosmic Visions: New Ideas in Dark Matter*, 7, 2017, [1707.04591](#).
- [47] LDMX collaboration, *Light Dark Matter eXperiment (LDMX)*, [1808.05219](#).
- [48] A. Berlin, N. Blinov, G. Krnjaic, P. Schuster and N. Toro, *Dark Matter, Millicharges, Axion and Scalar Particles, Gauge Bosons, and Other New Physics with LDMX*, *Phys. Rev. D* **99** (2019) 075001 [[1807.01730](#)].
- [49] H. An, M. Pospelov, J. Pradler and A. Ritz, *Directly Detecting MeV-scale Dark Matter via Solar Reflection*, *Phys. Rev. Lett.* **120** (2018) 141801 [[1708.03642](#)].
- [50] J. N. Bahcall, M. Pinsonneault and S. Basu, *Solar models: Current epoch and time dependences, neutrinos, and helioseismological properties*, *Astrophys. J.* **555** (2001) 990 [[astro-ph/0010346](#)].
- [51] E. Bulbul, M. Markevitch, A. Foster, R. K. Smith, M. Loewenstein and S. W. Randall, *Detection of An Unidentified Emission Line in the Stacked X-ray spectrum of Galaxy Clusters*, *Astrophys. J.* **789** (2014) 13 [[1402.2301](#)].
- [52] A. Boyarsky, O. Ruchayskiy, D. Iakubovskiy and J. Franse, *Unidentified Line in X-Ray Spectra of the Andromeda Galaxy and Perseus Galaxy Cluster*, *Phys. Rev. Lett.* **113** (2014) 251301 [[1402.4119](#)].
- [53] D. P. Finkbeiner and N. Weiner, *X-ray line from exciting dark matter*, *Phys. Rev. D* **94** (2016) 083002 [[1402.6671](#)].
- [54] F. D’Eramo, K. Hambleton, S. Profumo and T. Stefaniak, *Dark matter inelastic up-scattering with the interstellar plasma: A new source of x-ray lines, including at 3.5 keV*, *Phys. Rev. D* **93** (2016) 103011 [[1603.04859](#)].
- [55] J. Eby, P. J. Fox, R. Harnik and G. D. Kribs, *Luminous Signals of Inelastic Dark Matter in Large Detectors*, *JHEP* **09** (2019) 115 [[1904.09994](#)].
- [56] M. Pospelov, N. Weiner and I. Yavin, *Dark matter detection in two easy steps*, *Phys. Rev. D* **89** (2014) 055008 [[1312.1363](#)].

- [57] T. Lin and D. P. Finkbeiner, *Magnetic Inelastic Dark Matter: Directional Signals Without a Directional Detector*, *Phys. Rev. D* **83** (2011) 083510 [[1011.3052](#)].
- [58] CRESST collaboration, *First results from the CRESST-III low-mass dark matter program*, *Phys. Rev. D* **100** (2019) 102002 [[1904.00498](#)].
- [59] A. Moretti, S. Vattakunnel, P. Tozzi, R. Salvaterra, P. Severgnini, D. Fugazza et al., *Spectrum of the unresolved cosmic x-ray background: what is unresolved 50 years after its discovery*, *Astronomy & Astrophysics* **548** (2012) A87.
- [60] F. Perez and B. E. Granger, *IPython: A System for Interactive Scientific Computing*, *Computing in Science and Engineering* **9** (2007) 21.
- [61] T. Kluyver et al., *Jupyter notebooks - a publishing format for reproducible computational workflows*, in *ELPUB*, 2016.
- [62] J. D. Hunter, *Matplotlib: A 2d graphics environment*, *Computing In Science & Engineering* **9** (2007) 90.
- [63] S. van der Walt, S. C. Colbert and G. Varoquaux, *The NumPy Array: A Structure for Efficient Numerical Computation*, *Computing in Science and Engineering* **13** (2011) 22 [[1102.1523](#)].
- [64] M. Waskom et al., *mwaskom/seaborn: v0.8.1 (september 2017)*, Sept., 2017. [10.5281/zenodo.883859](#).
- [65] P. Virtanen et al., *SciPy 1.0: Fundamental Algorithms for Scientific Computing in Python*, *Nature Methods* (2020) .
- [66] C. O. da Costa-Luis, *tqdm: A fast, extensible progress meter for python and cli*, *JOSS* **4** (2019) 1277.